A Review Paper on

Applications of Frequency-Resolved Optical Spectroscopy in Nanoscience

By

Dileep Dhakal

Submitted to

Prof. Dr. Arnulf Materny

Principles and Applications of Optical Spectroscopy (200352)

December 2010

Abstract

Advancement of technology and development of high resolution optical elements, today optical spectroscopy has stood as the major analytical tool applied in every branch of science. This paper deals with two major applications of frequency resolved optical spectroscopy in the field of nanoscience- resonance Raman spectroscopy of single walled carbon nanotubes (SWCNTs) and photoluminescence (PL) spectroscopy of quantum dots (QDs).

CNTs have grown much attraction these days, being a novel and versatile material with very high tensile strength and electronically both semiconducting as well as metallic. SWCNTs can be generated by rolling a sheet of graphene (single atomic layer of graphite) at certain vector. Analysis of resonance Raman spectroscopy of SWCNT elucidates various features specific to both fullerene (C_{60}) family and sp^2 hybridized organic molecules. For example, SWCNT exhibits longitudinal and transverse optical phononic vibration mode (G band), radial breathing mode (RBM), G' band and D band. G band is common to all sp^2 hybridized organic molecules while RBM and G' band are present only in nanotubes.

QD are zero dimensional physical systems forming bridge between bulk and the atomic system. For example, presence of separate valence and conduction band similar to bulk system and discrete energy levels within the bands featuring atomic systems. Hence, spectroscopic behavior is similar to those of bulk as well as atomic system. PL spectroscopy of empty and charged quantum dots is discussed under different biasing condition. Biasing is necessary to lift the fermi level of dots to quantize the number of electrons inside the dot. Carrier confinement is proved observing the PL spectra of the quantum dots. Furthermore, growth dependent PL spectra of self assembled InGaAs QD is discussed. PL count is found to be narrow with high intensity peak for slowly deposited dots.

Table of Contents

1. Introduction to Optical Spectroscopy

Spectroscopy is the analysis of radiation after the interaction with the matter. Information about the matter is obtained from the modification of incoming electromagnetic radiation by the electronic and magnetic configuration of molecules.

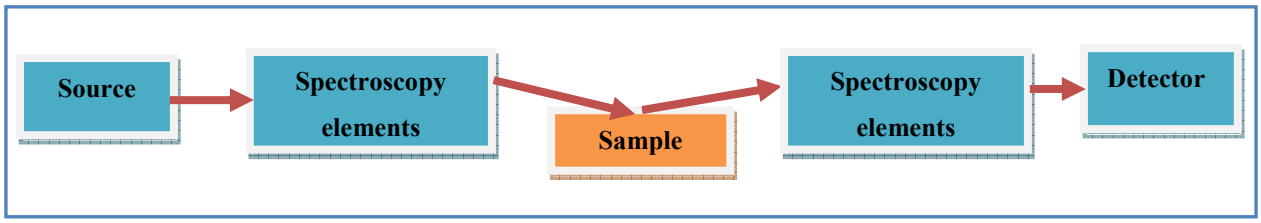

Figure 1

Schematic diagram of the spectroscopic technique.

The interaction between incoming radiations induces either excitation of particle to higher energy state termed as absorption or scattering process. The radiation involves can be any form either external electromagnetic or mechanical or internal embodied radiation within the matter. Electromagnetic radiation is widely applied radiation source in spectroscopy. It has a wide range of spectrum ranging from high energy gamma radiation to low energy radio waves (fig. 2).

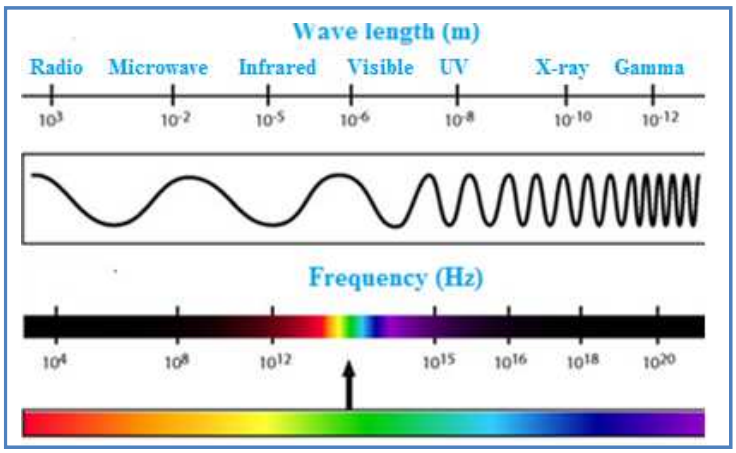

Figure 2

Typical electromagnetic spectrum- ranging between low energy radio waves and high energy gamma rays [1].

Optical spectroscopy deals with spectroscopic analysis involving any radiation source belonging to electromagnetic spectrum. When optical spectroscopic analysis is performed applying visible spectrum or ultra violet (UV) spectrum or infrared (IR) spectrum of X-ray it is termed as visible spectroscopy or UV spectroscopy or IR spectroscopy or X-Ray spectroscopy. Optical spectroscopy also involves light scattering: elastic scattering (energy of incoming radiation equals the scattered radiation) or inelastic scattering (energy of incoming radiation is different than the scattered radiation). Raman spectroscopy and Brillouin spectroscopy are typical inelastic scattering processes.

Optical spectroscopy can be carried out in frequency or energy domain, termed as frequency resolved spectroscopy (FRS) and in the time domain, termed as time resolved Spectroscopy (TRS). Relationship between different variables in FRS is expressed in the following equations:

$$E = h\,f \tag{1}$$

$$E = h\,\frac{c}{\lambda} = h\,c\,k \tag{2}$$

Where, E is the energy, f is the frequency, h is the Plank‘s constant, λ the wavelength, k the wave number and c is the velocity of light in vacuum.

Typical sources for optical spectroscopy are black body radiation (visible spectrum), gas discharge lamps (UV), spectral lamps (UV and visible), plasma emission (middle and far infra red) semiconductor lasers (wide range), and synchrotron (wide range). Optical elements used are optical filters, polarizers, phase plates, glass fibers, light pipes, monochromators, spectrometers, collimators and interferometers. Photomultipliers, CCD (Charged Coupled Devices) detectors, photographic films, photoelectric detectors, and photodiodes are the common detectors for optical spectroscopy. Spectroscopic technique has evolved as the versatile tool in the analysis of matter in every field of science which includes analysis of biomolecules, study of chemical reaction, detection of single molecule, study of transitional or vibrational or rotational spectra, study the properties of novel materials e.t.c. In the following section we would discuss two major applications of frequency-resolved optical spectroscopy in the field of nanoscience- Resonance Raman spectroscopy of single walled carbon nanotubes (SWCNTs) and photoluminescence spectroscopy of quantum dots (QDs)

2. Applications of Frequency Resolved spectroscopy

2.1 Resonance Raman Spectroscopy

Resonance Raman spectroscopy plays the significant role in understanding electron phonon interaction in sp^2 hybridized carbon systems. In resonance Raman spectroscopy, Raman process is combined with the optical absorption or emission. Hence, the combination enhances the Raman intensity by almost 1000 times [2]. Due to resonance Raman Effect it is possible to observe the phonon vibration modes of isolated single walled carbon nanotubes (SWCNTs). Frequency resolved spectroscopy is best when it turns in studying the resonance Raman spectra of fullerene (0D) or carbon nanotube (1D) or graphene (2D) or graphite (3D) structures, because phonon dispersion relation theoretically predicts the particular phonon vibration mode expected during the experiment (fig. 4).

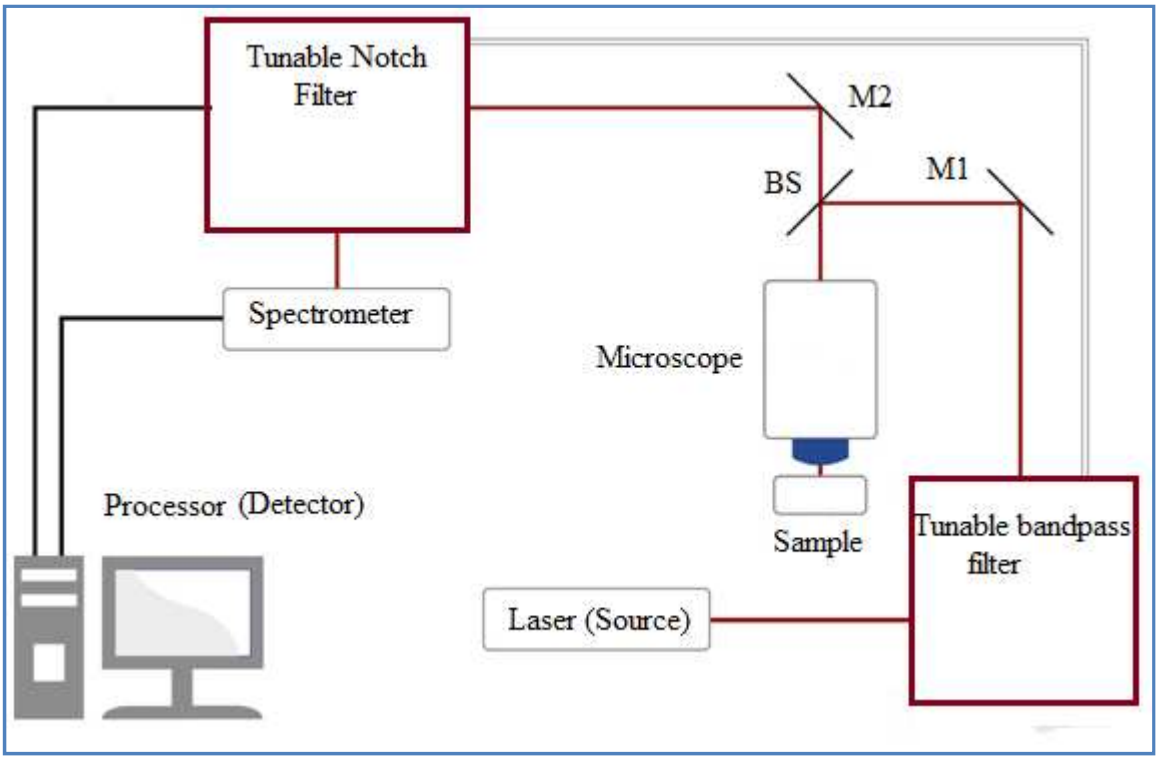

Figure 3

Basic schematic diagram for resonance Raman spectroscopy [1]. A laser is the typical excitation source applied to the sample. Scattered outgoing radiation is collected by the microscope. At the detector signal is passed through the notch filter to the processor.

Setup for resonance Raman spectroscopy is depicted in fig. 3. Laser (e.g. Ti-Sapphire) is the typical source of excitation applied to the sample. Monochromator is used to select certain frequency of excitation to the sample. Sample will then scatter the incoming signal, which is collected by the microscope. A microscope then gathers all scattered outgoing signal from the sample and the signal is fed to the beam splitter (BS). From BS it is applied to the processor. Major advantage of having notch filter before processor is to neglect Rayleigh scattered radiation from the sample.

Single Walled Carbon Nanotube (SWCNT)

CNT is an allotrope of carbon with cylindrical structure and can be single walled or multi-walled. Different direction of rolling a graphene sheet yields modulation of the electrical property of CNT, yielding either semiconducting or metallic property. A SWCNT is prepared by rolling a single graphene sheet (each carbon atom is bonded with three other carbon atoms with sp^2 hybridization forming a closed hexagonal structure) along a certain vector direction termed as chiral vector (C_h) (fig. 4). On electron is always free to move along the plane of carbon hexagon ring in every allotropes of carbon derived from graphene.

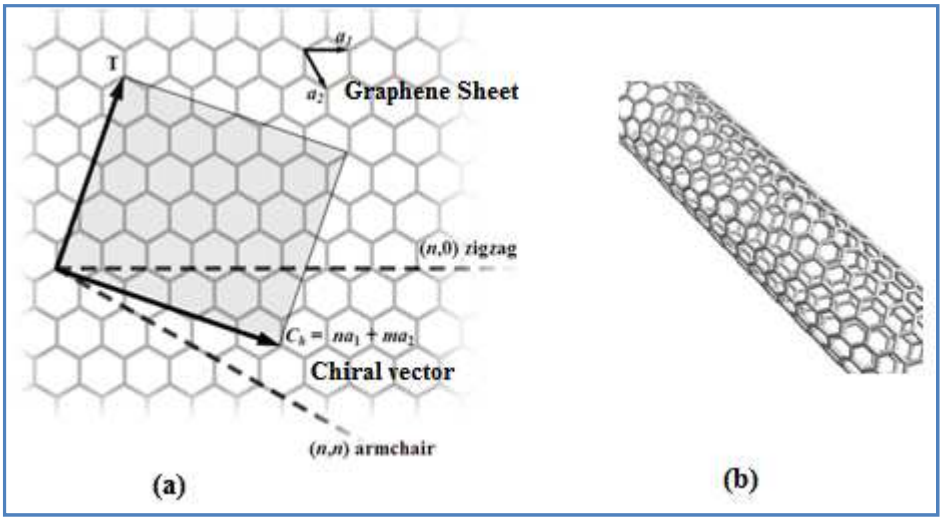

Figure 4

(a) Rolling a graphene sheet along the chiral vector C_h (n, m) to get SWCNT. (b) A typical SWCNT for C_h (n, n) [3]. For different chiral vector different CNTs are obtained: for zigzag (n, 0) we obtain semiconducting and for armchair (n, n) we obtain metallic CNTs) [4].

Phonon dispersion relation in graphene

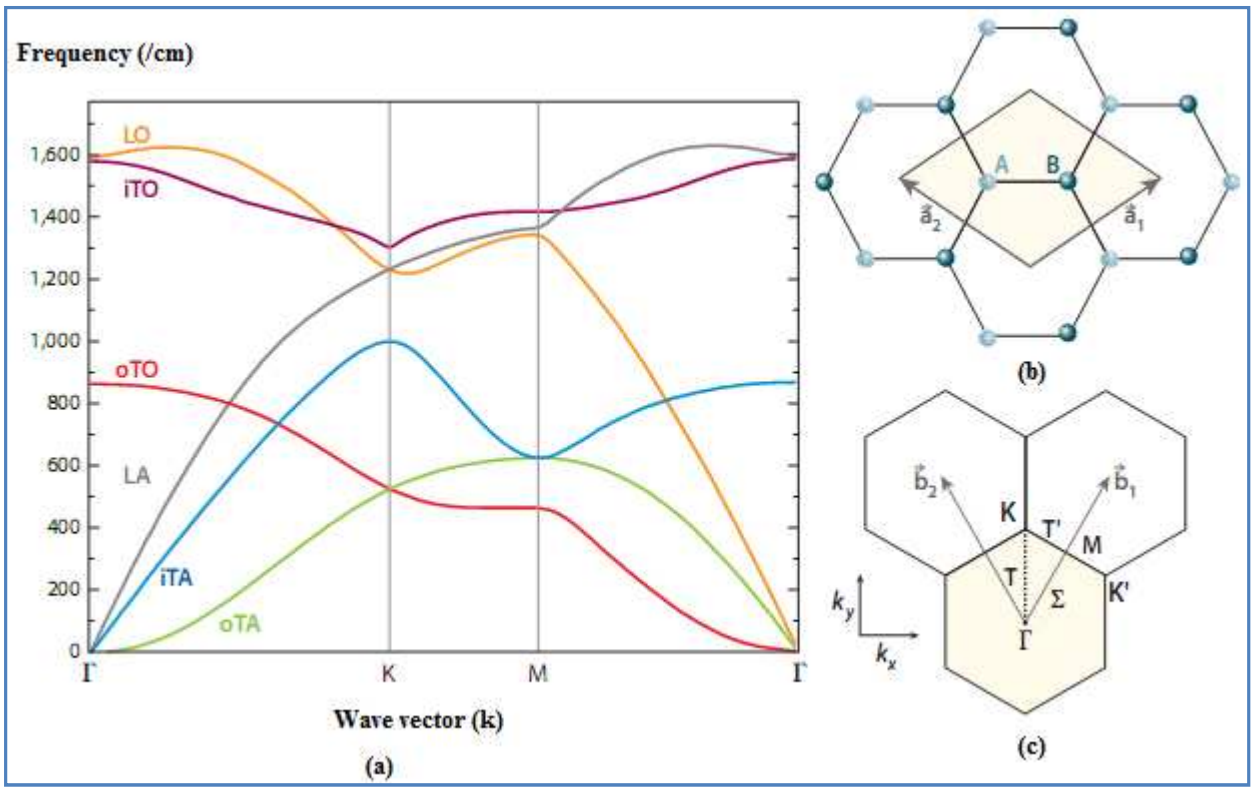

Figure 5

(a) Phonon dispersion relation of a single layer of graphene (SLG) structure, showing LO, iTO, oTO, LA, iTA, oTA phonon modes [3]. (b) Real space lattice of SLG structure, A and B are corresponding nearest atoms displaced by 0.142nm. (c) Reciprocal lattice of SLG showing respective first Brillouin zone (BZ) with highly symmetric points- Γ (centre of the first Brillouin zone (BZ)) and K (centre of edge joining two hexagonal faces of the BZ) points of the SLG structure [3].

Phonon dispersion relation of graphene (sp^2 hybridized state) must be clearly understood before interpreting the Raman spectra of CNTs. Since first BZ of graphene consists of two atoms (fig. 5(c)); hence, six phononic dispersion branches are expected in these materials. From calculated phonon dispersion relation of graphene in fig. 5, we can clearly observe three optical phonon branches and three acoustic branches. Each three transverse mode of vibration-perpendicular to the direction of wave vector (k) optical and acoustic phonon branches is whether in plane (i) or out of plane (o). The remaining three longitudinal modes are associated with the vibration of atoms parallel with the wave vector. In phonon dispersion relation, Γ and K point are the major

point of interest. Here, we observe both LO and TO phonons degenerates at q=0 (Γ point) but at q=K point they are non-degenerate. Thus, at K-point longitudinal electric field contributes more for optical phonons. Additionally, at K point oTO - oTA and LO - LA degenerates giving doubly degenerated phonons (Fig 5(a)).

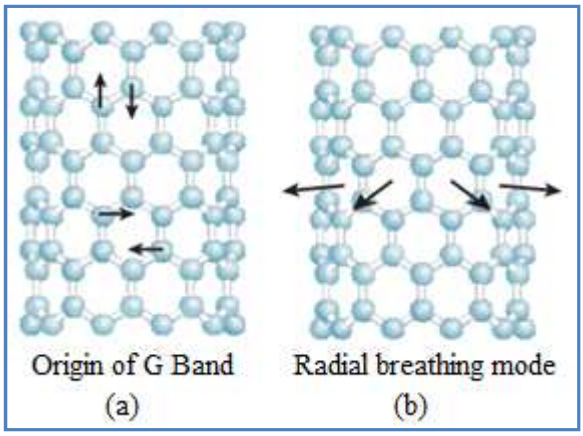

Figure 6

C-C bond stretching in CNTs– origin of G-Band (a) or radial breathing mode (RBM) (b) due to radial vibration of each CNT atom [3].

Resonance Raman spectroscopy of SWCNT

When a SWCNT is illuminate with a laser source of 2.414 eV, we observe the following four major band associated with different phonon vibration modes-G, G', D and RBM (fig. 7). As discussed in phonon dispersion relation (fig. 5(a)), G-band (at 1593/cm in fig. 7) in SWCNT is composed of six different vibration modes of carbon atoms- vibrating along the tangential direction with respect to the tube surface, is composed of three modes along the tube axis (LO) and other three modes along the circumference (TO) of the tube (fig. 6). Furthermore, SWCNT exhibits two other dominating Raman spectra under resonance condition [3], radial breathing mode at 186/cm and the G' band (at slightly lower energy (1567/cm) compared with that of G band (fig. 7)).

D band also termed as defect band is the indication of presence of defects in SWCNT samples, which depends on the excitation energy and takes place at 1350/cm for 2.414eV laser source, and

present in all allotropes of carbon with sp^2 and sp^3 hybridization [3]. Careful comparison of D band for different CNT samples would be an indicator of defects in CNTs.

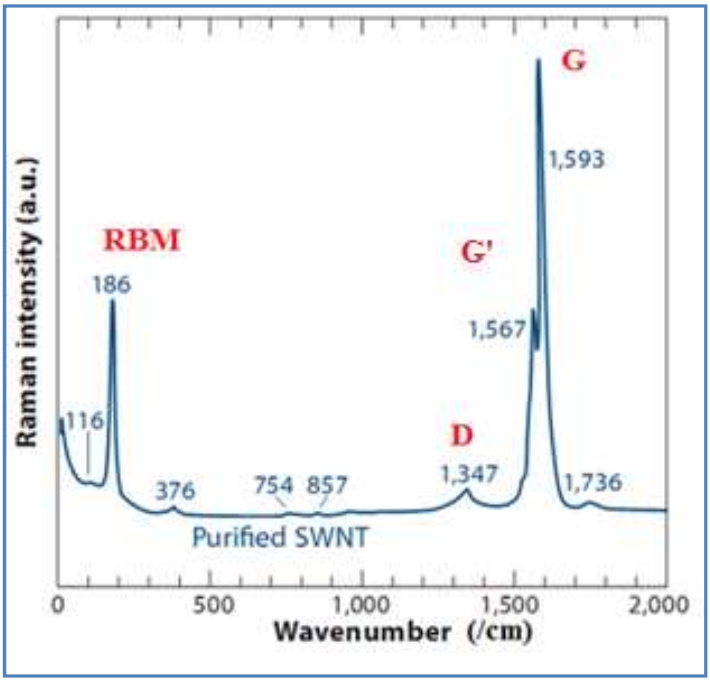

Figure 7

Resonance Raman spectra of purified SWCNT (grown by laser vaporization method), depicting different phonon vibration modes [3]. Hence, we can observe G and G' band around 1580 /cm, RBM at 186 /cm and disorder mode (D) at 1347/cm.

RBM is only present in CNTs, they proves the presence of nanotubes compared with graphene where this peak is absent. Additionally, Radial breathing mode frequency (w_{RBM}) is inversely dependence on the tube diameter (d_t) [4]. By analyzing the radial breathing mode frequency we can differentiate CNTs with different diameter and also measure the diameter of tube.

$$w_{RBM} \propto \frac{1}{d_t} \tag{3}$$

In fig. 8, three forms of graphene structures are compared- neutral graphite (multi layered graphene), metallic SWCNT and semiconducting SWCNT. G' band is variable in all these structures while G band is common to them. The G' band in resonance Raman spectra is narrow

with sharp peak for semiconducting CNT compared to metallic where it is broad, and absent in the case of graphite. Thus, G' band would be a good indicator for detecting electronic property of SWCNTs.

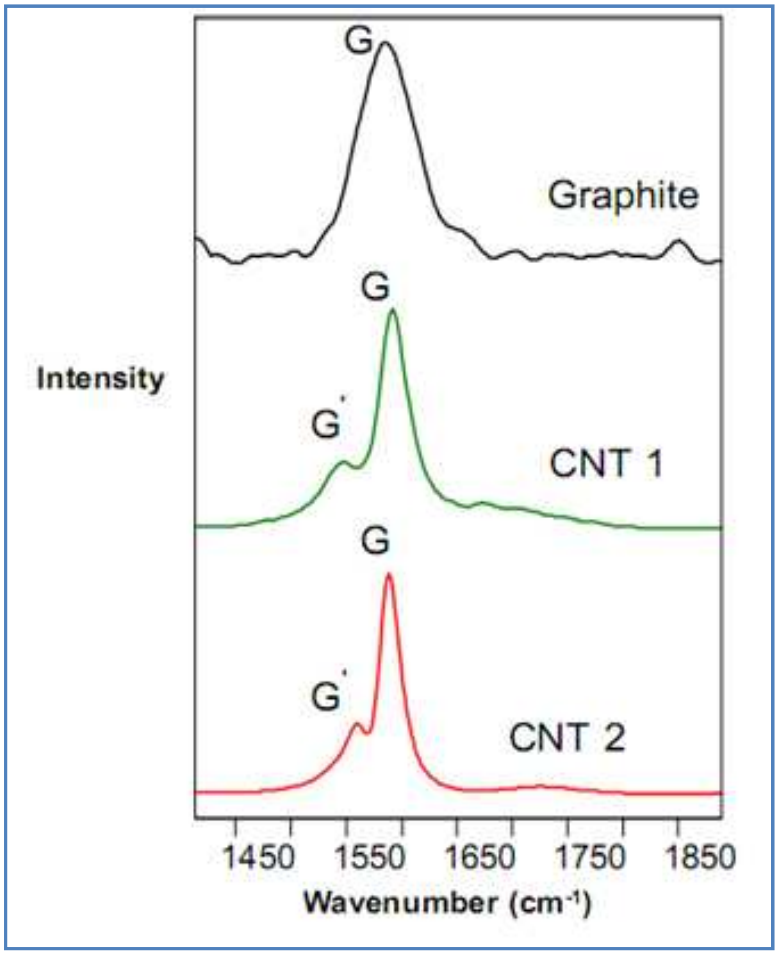

Figure 8

Resonance Raman spectra for Graphite (neutral), metallic CNT (CNT1) and semiconducting CNT (CNT2) [5].

2.2 Photoluminescence Spectroscopy of Quantum Dots

Photoluminescence (PL) involves excitation of a particle to higher energy state by applying photon of radiation, and on returning to ground state system emits photon radiation. Similar process for chemical substance is termed as fluorescence, where a molecule is excited to higher energy states (absorption), then it relaxes to stable state, and returns to ground state emitting a radiation with energy less than the excitation radiation termed (typical red shift). Technically, electric field induced excitation is termed as electroluminescence, is the electric potential induced excitation of particle to higher energy state, and on returning to ground state energy equal to the excitation is emitted giving luminous intensity. In semiconductor, when electrons are excited to conduction band, they leave holes behind on valence band. Thus, generated electron-hole pair is termed as an exciton pair. LASER is typical source of excitation for PL spectroscopy. Photomultiplier tubes and CCDs are widely used PL detectors.

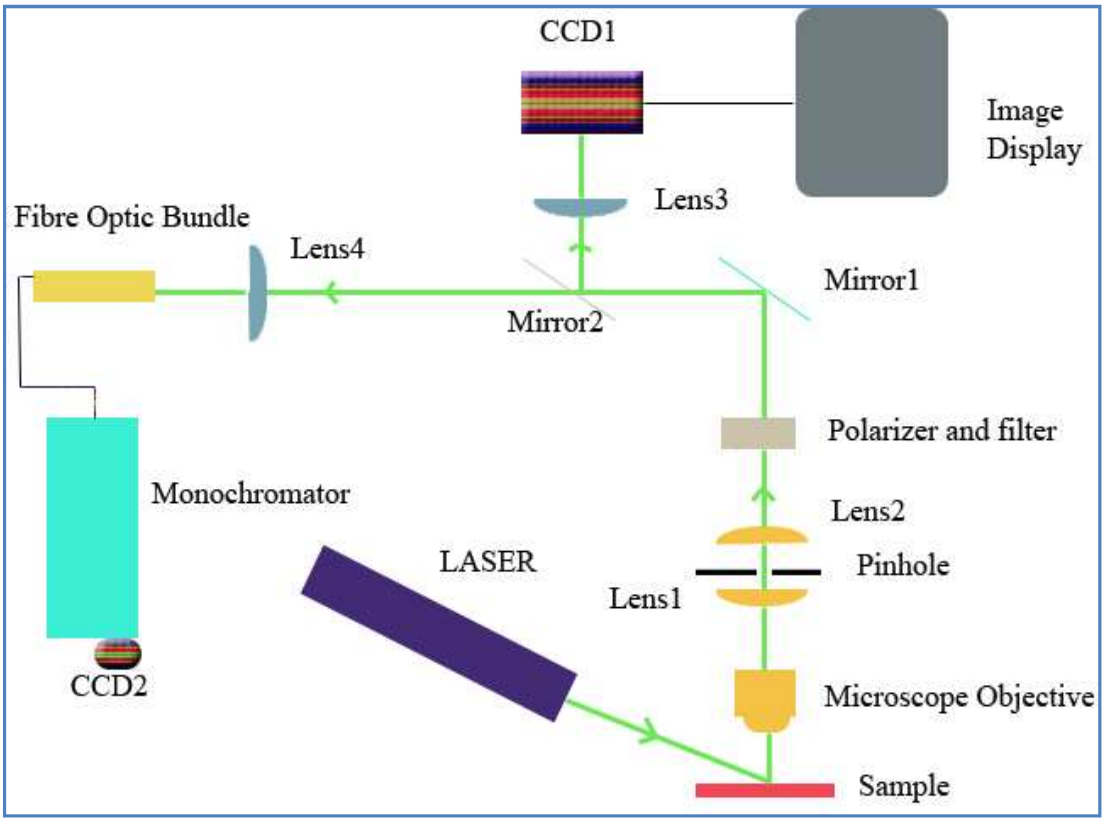

Figure 9

Experimental setup for Photoluminescence spectroscopy. Sample and CCD must be placed inside the cryogenic environment to prevent any unwanted excitation, will reduce the noise [2].

The luminous intensity generated after recombination of exciton is collected by the microscope objective lens. Microscope is used to access small region of the sample. Outgoing radiation is then sent to the filter and the polarizer. Before feeding to the filters, outgoing radiation is always applied through a pinhole for the removal of background noise. Finally, outgoing radiation is sent to half polished mirror to the CCD detector and then to the processor.

Introduction to Quantum dots

When electron is excited by energy of sufficient radiation, electron jumps to an excited state (with energy equal to the difference of excited state and the ground state). In the bulk system, electron jumps to conduction band (CB) leaving a hold behind in valence band (VB) when energy is greater than the band gap (E_g) in fig. 11. CB is empty and VB is filled states (at T=0K), are regions with high density of states compared with the band gap with no available states for occupation.

$$E_g = E_c - E_v \tag{4}$$

Bohr radius of exciton is the physical representation of distance (r) in the crystal when, electron leaves the hole in the valence band and reach the conduction band. Now, when the size of the device is decreased such that it is much smaller than the Bohr radius of exciton, band gap size of is then influenced by the kinetic energy of the particles (eq. 5).

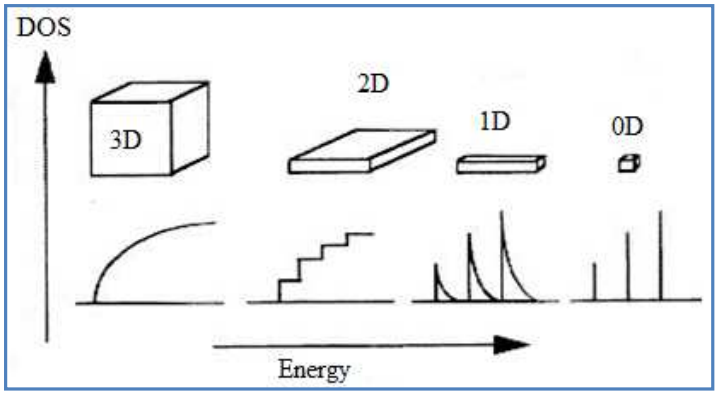

Figure 10

Density of states (DOS) vs. energy in 0D, 1D, 2D and 3D systems. Compared to 3D system, where DOS exponentially increases with energy, in QDs or 0D structures we observe discrete energy levels [6].

Mathematically, difference between the ground state (HOMO-Highest Occupied Molecular Orbital) and the first excited state (LUMO-Lowest Unoccupied Molecular Orbital) in quantum dot is given by the equation (5) [7]:

$$E_{1s-1s} = E_{gap} + \frac{h^2\left(n_1^2+n_2^2+n_3^2\right)}{2m_e^* d^2} + \frac{h^2\left(n_1^2+n_2^2+n_3^2\right)}{2m_h^* d^2} - \frac{e^2}{8r\pi\varepsilon} \quad (5)$$

Where, h is Planck's constant,

n is quantum number,

m is corresponding reduced mass (m_e* is for electron and m_h^* is for hole),

ε is dielectric property of the QD

d is the size of the QD,

r is the separation distance between electrons and holes.

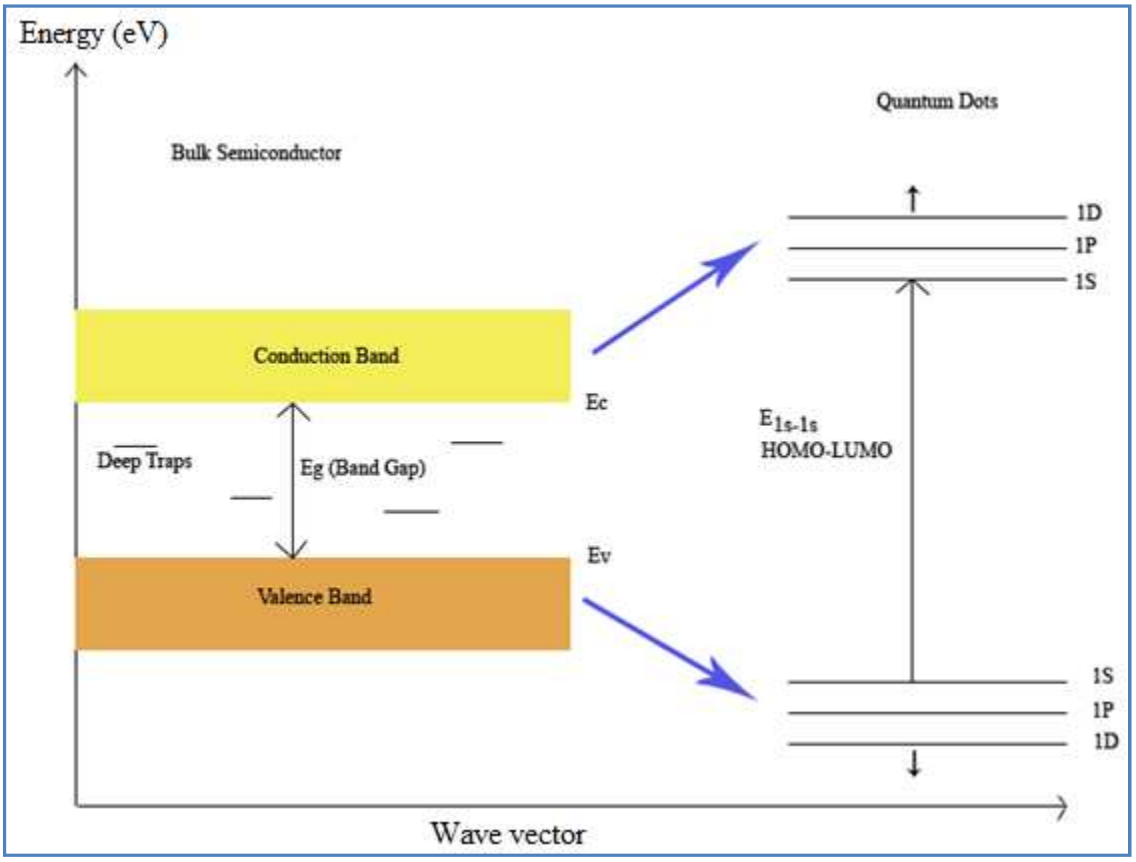

Figure 11

Energy diagram for bulk system (left) and a quantum dot (right). E_c and E_v are corresponding conduction and valence band edges [7].

From equation (5), with increasing r (Bohr's radius of exciton) and decreasing device size (d), the kinetic energy term is hence increased, resulting in discrete energy levels. Compares with bulk system band gap is shifted towards the blue energy. Thus, the difference between ground state and the first excited state (E_{1s-1s}^{QD}) > E_{gap}^{bulk}) in QD is greater than the band gap of bulk system (E_{gap}^{bulk}). Band gap of QD depends on the corresponding quantum numbers (n) and the respective effective mass of electrons (m_e^*) and holes (m_h^*).

Discrete energy level in QDs:

$$DOS_{0D} = \sum_{En<E} \delta(E - E_n) \tag{6}$$

Quantum dots are the 0D structures and exhibits quantized density of states for certain energy level, mathematically expressed by equation (6). From fig. 11, we can observe that when dimension of the system decreases, more the system exhibits quantized behavior. Hence, a QD exhibits a confinement of the carrier, and the energy of the particle in any state depends on the quantum number. Spectroscopically, such system much exhibit sharp peak in the intensity. Fig. 12 depicts the quantization of state in an empty QD with sharp peak in the intensity, when a quantum dot is excited with the laser pulse.

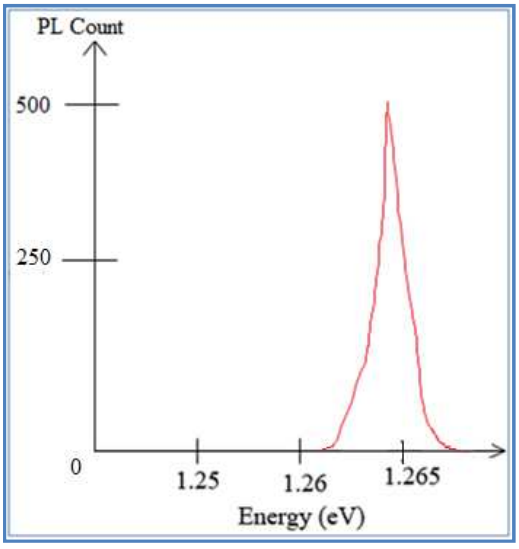

Figure 12

PL spectra of InAs QD in GaAs layer, pumped by laser diode (822nm, 1μW) at 4.3K with -0.76V as gate voltage.

Coulombs Blockade

Is the phenomenon in nanoscopic system, where an electron opposes the filling of additional electron by Coulombs repulsion, takes place only at very low temperature. The resistance of such system is very high after addition of first electron, since capacitance increases with addition of multiple electrons. Additional energy is required to overcome the repulsive force between the electrons in reservoir and QD is termed as charging energy.

Figure 13

(Left) Addition of first electron to an empty QD. (Right) Addition of second electron to the charged QD.

Subsequent additions of electrons are always easier because capacitance of the dot increases with increase in number of electrons in the QD.

$$\text{Charging Energy: } E_c = \frac{e^2}{C} \gg K_B * T \qquad (7)$$

$$= 25\text{meV at } 300\text{K}$$

Where, e = $1.6 * 10^{-19}$ Coulomb,

T = Absolute temperature,

K_B = Boltzmann's constant,

C = Capacitance between the dot and reservoir

Hence, charged quantum dot must exhibit red shift in the peak intensity for subsequent addition of electrons.

Growth of Quantum dots

A basic QD (InAs QD in GaAs) band diagram is depicted in the fig. 13, where band gap of QD (InAs) is much smaller than the GaAs. Thus, GaAs acts as the tunnel barrier which opposes the flow of carrier from the reservoir (external potential source) creating huge potential barrier outside the dot.

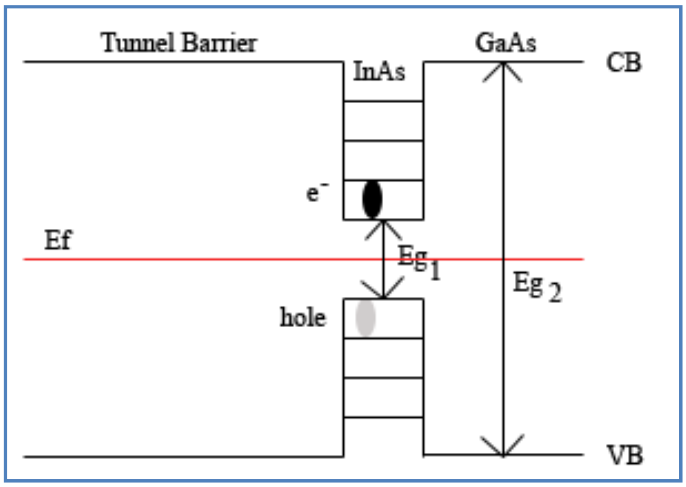

Figure 14

QD diagram (E_{g1}=1.348eV, E_{g2}=0.38eV), CB is conduction band and VB is valence band edge and E_f is fermi energy level. GaAs acts as the barrier preventing the flow of carrier in dot [7].

QDs can be growth by the process termed as self assembled growth, where very high concentration of QDs can be deposited by molecular beam epitaxy technique, will be discussed in further section.

a. Uncontrolled QD growth process

Crystal growth during MBE takes place by either layer by layer or layer and island growth. Strain between lattices during deposition results in high diffusion length of deposited molecules forming layer and layer growth. While strained system must result in low diffusion length resulting in layer and island growth. When, InAs is grown on GaAs layer, lattice mismatch between GaAs and InAs results in strain within the lattice, resulting in the formation of small island of InAs above the GaAs layer. Since, lattice constant of GaAs (5.65 A°) is smaller than

InAs (6.0584 A°), GaAs goes strained and in reverse, InAs goes compressed. Deposited QD size cannot be controlled (fig. 15) in this process.

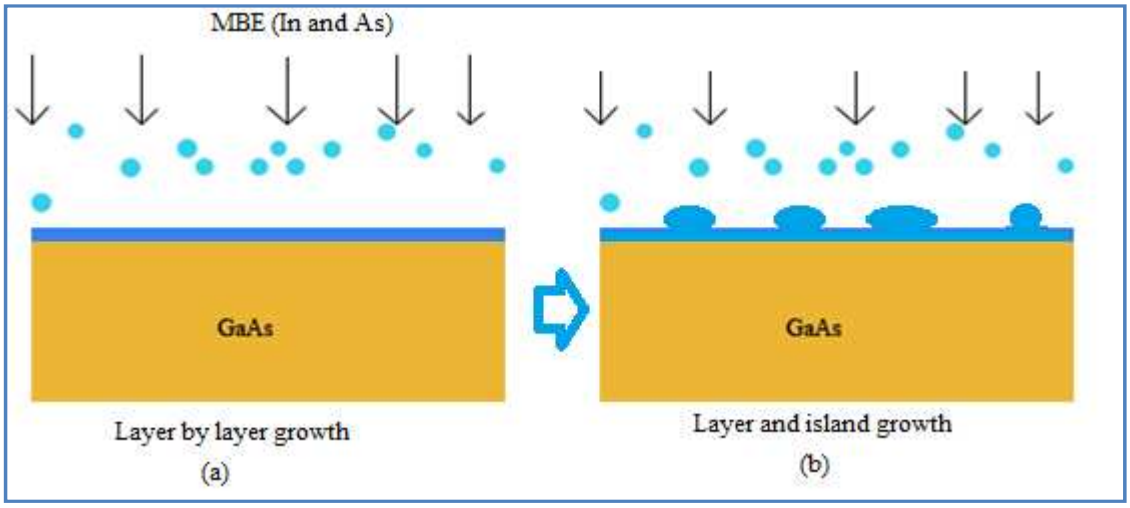

Figure 15

(a) Molecular Beam Epitaxial (MBE) layer growth of Indium (In) and Arsenic (As) ions on the GaAs layer, initial phase. (b) Formation of InAs islands with varying QD area [9], depicting layer and island growth.

b. Controlled Mode

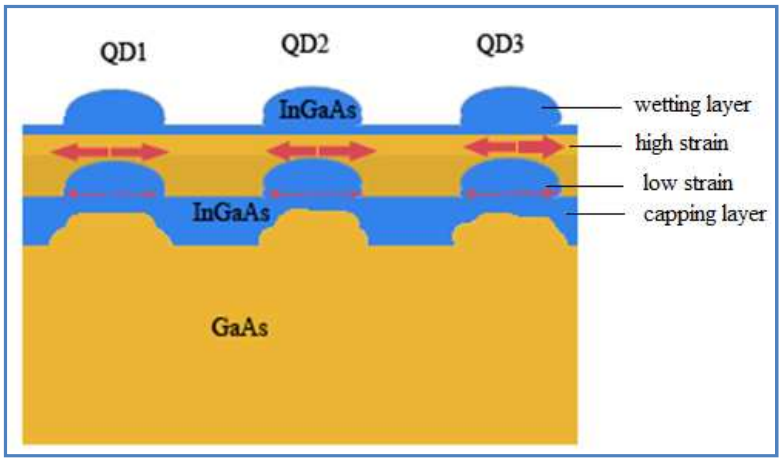

Figure 16

Controlled self-assembled QDs (InGaAs) grown on the GaAs, InGaAs is a capping layer between two GaAs layers. QDs or wetting layers grows exactly above the caps of the capping layer [7].

By applying a capping layer of InGaAs inside the GaAs layer, we precisely control the region of high and low stress [9]. Thus, after MBE we get nucleated QD (wetting layer) grown exactly at those regions above the capping layer. Is the controlled and widely applied Self assembled (SA) QD growth process.

Growth PL Spectroscopy of QD

PL spectroscopies of QDs are observed for different deposition rate to understand the dependency of quantum dot emission with the dot size. When quantum dots are grown for different deposition rate, size of the individual dots would vary. Slowly deposited would have large size compared with quickly deposited dots. Larger is the dot size more the emission peak must shift towards lower energy (red shift). In fig. 17, when dots were deposited with decrease in the rate of deposition from 0.5 to 0.0065 ML/s, the peak of the emission is increasing towards lower energy.

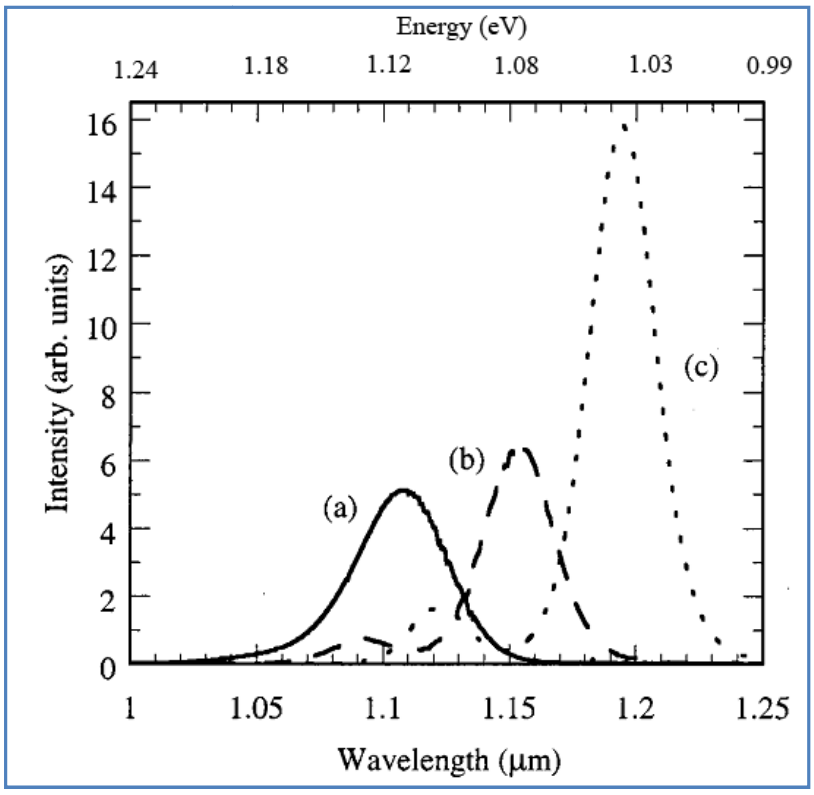

Figure 17

PL spectra for Quantum dots 2.2ML of InAs deposited at 10K, with wetting layer deposition rate is varied from (a) 0.55 (b) 0.016 (c) 0.0065 ML/s and capping layer is deposited with 2.7ML at 490°C [8].

The reason behind shifting of peak (fig. 17), with slow deposition rate is increase in the volume of the dot. For larger dot size photoluminescence must take place at lower energy (eq. 5) - typical red shift. Physically, increases in intensity for slowly deposited dots are due to the presence of higher percentage of indium ions.

PL spectroscopy of charged and neutral QD

Single electron storage has always been great interest for scientist from all over the world due to its greater advantage in storing the quantum information in the form of electron spin inside the QDs [2]. Recently, a biexction recombination has been successfully experimented for the generation of entangled photon pair inside the InGaAs single quantum dots [10].

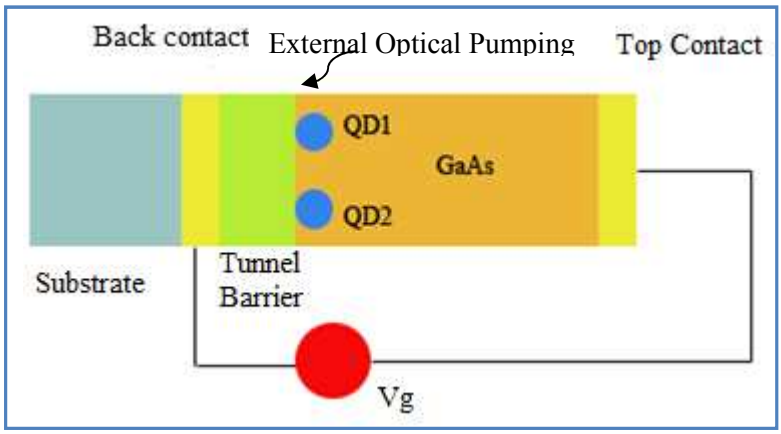

Figure 18

A quantum dot structure connected with external biasing source (Vg). Vg is applied between back contact and the top contact to precisely control the number of electrons going in and out of the dot. InAs QD fabricated in GaAs with 25nm tunneling barrier is fabricated. Experiment was carried Using laser diode at1μW pumping power emitting in 822nm at 4.2K [9].

To electrically characterize the QD, an external biasing potential must be applied to the QD between the contacts. External bias potential will precisely control the number of electrons entering inside the quantum dots. Constant optical pumping ensures generation of exciton pair

which recombines to yield photoluminescence spectra which is measured at the detector. We would expect certain atomic behavior in the spectroscopy of quantum dot analogous as the spectroscopy of hydrogen atom.

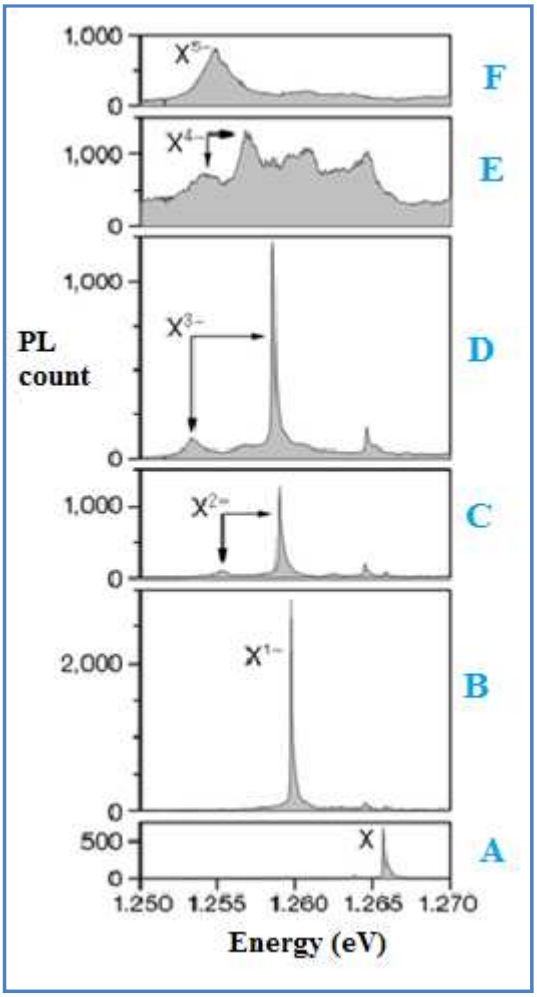

Figure 19

Spectroscopy of a charged and neutral QD. In each step an electron is added to the dot and the respective photoluminescence spectra is recorded (spectra A to F) [9].

In fig. 18 changing the gate voltage, we can shift the fermi level heterostructure and control the number of electrons going into the dot. At very low gate voltage (Vg=-0.76V) we get ground state exciton recombination within an empty QD, results in small PL count- order of only 500 (A), taking place at higher energy of optical-excitation. When gate potential is increased to -0.16V (B), first electron enters the quantum dot- due to shift in Fermi energy level. Due to optical pump source and external bias, electrons and holes recombine to give sharp increase in

the PL Spectra (nearly 2500-spectra B). Thus, QD is charged. Now, addition of second electron to the dot is very difficult, which result in low intensity of PL count. Additionally, two electrons in any energy levels within the quantum dot could be quantum mechanically in either singlet state (total spin is 0) or triplet state (total spin equals 1). Spectra (C) is composed of two intensity peak; one at higher energy level, is a singlet state for two electron quantum dot and second satellite peak with low PL intensity is an unfavorable triplet state, at low energy of excitation. Additionally, the peak intensity also depends on the electron-electron correlation in multielectronic QDs. In multielectronic QDs broad PL spectrum is observed (Spectra E and F).

Following equation 7, charging energy decreases with subsequent addition of electron above two electrons compared with two electrons in the QD. Hence, maximum of PL spectra takes place at lower energy of optical excitation. Thus, we can clearly observe red shift in the PL spectrum in fig. 19 (A to H).

Conclusion

The basic aspects of the frequency resolved optical spectroscopy in the field of nanoscience has been successfully reviewed by discussing major applications in nanoscience- spectroscopy of SWCNTs and spectroscopy of QDs.

Resonance Raman spectroscopy of SWCNT was found to be similar to those of sp^2 hybridized carbon compounds esp. due to the presence of G band, common to graphene and CNTs (fig. 7). Additionally, several CNT specific properties were obtained by resonance Raman spectroscopy like, radial breathing mode and the presence of G' band. Radial breathing mode frequency could be used in comparing CNTs with different diameters. Similarly, comparison of G' band for different CNTs would be a good indicator for the presence of either metallic or semiconducting CNT (fig. 8).

Quantum dots are the physical system lying between atomic and bulk systems. Hence, they exhibit both band structure similar to those of bulk system as well as discrete band structures similar to those of atomic systems. PL spectra of QD system is found to be a sharp delta peak like feature when excited with a suitable laser source (fig. 12). PL Spectroscopy of quantum dot grown by self assembly for different deposition rate was then discussed. Slowly deposited dots (at 0.0065 ML/min) were found to be superior compared with quickly (0.05 ML/min) deposited dots (fig. 17). Firstly, amount of arsenic and indium atoms were quite high in slowly deposited QDs resulting in both narrow and high intensity peak of luminescence. Secondly, size of slowly deposited dots were larger compared with quickly deposited, giving red shift in absorption peak.

Furthermore, carrier confinement in quantum dots were observed by careful analysis of quantum dot PL spectroscopy under biased condition. Red shift in the spectrum (fig. 19) is quite good indicator for the presence of electrons in the dot. Also, electron hole recombination is favorable for increased gate potential with increase in the number of electrons in the dot. Interesting fact observed was they exhibit sharp peaks as similar to those of atoms and the spectrum gets broader with increase in the number of electrons stored in the QDs (fig. 19) – featuring both atoms and bulk system.

References

[1] http://www.kollewin.com/EX/09-15-03/electromagnetic-spectrum.jpg

[2] Hans Kurzmany, '*Solid State Spectroscopy*', Springer 2009

[3] M. S. Dresselhaus, A. Jorio, R. Saito, '*Characterizing Graphene, Graphite and Carbon Nanotubes by Raman Spectroscopy*', Ann. Rev. Cond. Mat. Phy., 1, 89-108 (2010)

[4] http://www.seas.upenn.edu/mse/research/nanotubes.html

[5] Costa S.**,** E. Borowiak-Palen, M. Kruszyñska, A. Bachmatiuk, R J. Kaleńczuk, '*Characterization of Carbon Nanotubes by Raman Spectroscopy,'* Mat. Sci. Pol. 26 (2), 433-441 (2008)

[6] S. Bandyopadhyay, H. S. Nalya, '*Quantum Dots and Nanowires*,' American Scientific Publishers (2003)

[7] P. Michler, '*Single Quantum Dots-Fundamentals, Applications and New Concepts*,' Springer (2003)

[8] P. B. Joyce, T. J. Krzyzewski, G. R. Bell, and T. S. Jones, '*Effect of growth rate on the size, composition, and optical properties of InAs GaAs quantum dots grown by molecular-beam epitaxy*', Phy. Rev. B, Vol. 62, No. 16 (2000)

[9] R. J. Warburton, C. Schäflein, D. Haft, F. Bickel, A. Lorke, K. Karrai, J. M. Garcia, W. Schoenfeld, and P. M. Petroff, '*Optical emission from a charge-tunable quantum ring*', Nat. 405, 926-929 (22 June 2000)

[10] C. L. Salter, R. M. Stevenson, I. Farrer, C. A. Nicoll, D. A. Ritchie, A. J. Shields, *'An entangled-light-emitting diode*,' Nat. 465 (June 2010)